Intramolecular Two-Electron Transfer between Manganese(II) and Semiquinone Ligands. Synthesis and Characterization of Manganese 3,5-Di-*tert*-butylquinone Complexes and Their Relationship to the Photosynthetic Water Oxidation System

Michael W. Lynch,[1a] David N. Hendrickson,*[1a] Brian J. Fitzgerald,[1b] and Cortlandt G. Pierpont*[1b]

Contribution from the School of Chemical Sciences, University of Illinois, Urbana, Illinois 61801, and the Department of Chemistry, University of Colorado, Boulder, Colorado 80309. *Received May 16, 1983*

Abstract: Synthetic procedures for preparing the green $Mn_4(3,5\text{-DBSQ})_8$ tetramer are reported. Spectral and structural characterization of the complex shows that the metal ions are in the Mn(II) form and that the quinone ligands are bonded as semiquinones. Weak magnetic exchange between the high-spin d^5 metal ions and the paramagnetic ligands results in a magnetic moment of 5.1 μ_B per $Mn(3,5\text{-DBSQ})_2$ unit at room temperature. Treatment of the tetramer with pyridine results in formation of the $Mn(3,5\text{-DBCat})_2(py)_2$ monomeric addition product. A structural study has shown that the metal ion of this molecule is Mn(IV) and that the quinone ligands are bonded in their catecholate form. EPR spectra verify the d^3 configuration of the metal ion. In toluene solution at room temperature purple crystals of the complex give a green solution. At temperatures below 230 K the solution assumes the purple color of the crystals. Spectral evidence suggests an equilibrium between $Mn^{II}(3,4\text{-DBSQ})_2(py)_2$ (green) and $Mn^{IV}(3,4\text{-DBCat})_2(py)_2$ (purple) forms of the complex over the temperature range between 230 and 300 K in toluene. In pyridine the equilibrium temperature range is increased by approximately 100 K. The physical and structural properties of the manganese complexes are compared with the properties of the manganese protein associated with photosynthetic water oxidation.

Recent interest in the development of photocatalysts for water oxidation has been primarily directed at oxides of platinum group metals in heterogeneous systems[2] and ruthenium–bipyridine complexes in homogeneous media.[3] It is somewhat surprising that greater effort has not been devoted to investigations on model systems for biological photosynthetic water oxidation. Products of the process are molecular oxygen and charge for photosystem II (PSII) of the photosynthetic unit.[4] A model first suggested by Kok in 1970 based on O_2 flash yield kinetics[5] describes this process in terms of four sequential photooxidation steps of two water molecules bonded at the active site of a protein catalyst. Four manganese ions are located at this site and are required for oxidation.[6] Two of the manganese ions can be easily extracted from the enzyme with Tris or NH_4OH or by heating and are obtained in the form of Mn(II).[7] Inhibition of O_2 evolution and the associated light reactions of PSII upon extraction of the "loosely bound" manganese led to the view that these metal ions were directly associated with the water oxidation process. More recent work has shown that O_2 evolution continues in the absence of extractable manganese[8] and that replacement of these metal ions with other divalent ions (Mg^{2+}) restores electron transport in PSII.[9] The current view is that the "loosely bound" manganese ions serve in a secondary function, possibly maintaining an important conformational structure for the protein, and that the two "firmly bound" Mn ions are actively involved with water oxidation.[9] Sauer and Wydrzynski have described a model for O_2 production with a bimetallic $\langle Mn^{2+},Mn^{2+}\rangle$ site, which, as a unit, can undergo reversible changes in oxidation state and places the oxygen atoms in close proximity to facilitate O–O bond formation.[10] EXAFS studies suggest a Mn–Mn separation of 2.7 Å and an inner coordination sphere for the metal ions consisting of "light" donor atoms (O and N) but not a porphyrin ring. The mixed-valence Mn^{III},Mn^{IV} dimer I containing bipyridine ligands appears to bear

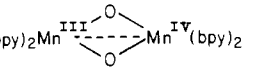

I

a structural similarity to the biological bimetallic site.[11,12] In particular, the Mn–Mn separation of 2.72 Å is nearly identical with the results of the EXAFS study, and the EPR spectrum of I has features in common with the spectrum of the photosynthetic complex.[13]

Perhaps the best functional model for the chemistry associated with the manganese protein has been reported by Meyer and co-workers for a bimetallic ruthenium complex.[14] In this scheme (eq 1) a Ru(III) dimer undergoes oxidation by either chemical or electrochemical means to produce O_2 from two coordinated

(1) (a) University of Illinois. (b) University of Colorado.
(2) (a) Humphry-Baker, R.; Lilie, J.; Grätzel, M. *J. Am. Chem. Soc.* **1982**, *104*, 422–425. (b) Collin, J. P.; Lehn, J. M.; Ziessel, R. *Nouv. J. Chim.* **1982**, *6*, 405–410. (c) Shafirovich, V. Ya.; Strelets, V. V. *Ibid.* **1982**, *6*, 183–186.
(3) (a) Sutin, N.; Creutz, C. *Pure Appl. Chem.* **1980**, *52*, 2717. (b) Nijs, H.; Cruz, M. I.; Fripiat, J. J.; Van Damme, H. *Nouv. J. Chim.* **1982**, *6*, 551–557.
(4) (a) Sauer, K. *Acc. Chem. Res.* **1980**, *13*, 249–256. (b) Bouges-Bocquet, B. *Biochim. Biophys. Acta* **1980**, *594*, 85–105. (c) Wydrzynski, T.; Sauer, K. *Ibid.* **1980**, *589*, 56–70.
(5) Kok, B.; Forbish, B.; McGloin, M. *Photochem. Photobiol.* **1970**, *11*, 457–475.
(6) (a) Chemiae, G. M.; Martin, M. *Biochim. Biophys. Acta* **1970**, *197*, 219–239. (b) Radmer, R.; Chemiae, G. M. *Top. Photosynth.* **1977**, *18* 303–348. (c) Chemiae, G. *Methods Enzymol.* **1980**, *69*, 349–363. (d) Dismuke, G. C.; Ferris, K.; Watnick, P. *Photobiochem. Photobiophys.* **1982**, *3*, 243–256.
(7) Klimov, V. V.; Allakhverdiev, S. I.; Shuvalov, V. A.; Krasnovsky, A. A. *Dokl. Akad. Nauk SSSR* **1982**, *263*, 1001–1005.
(8) Mansfield, R.; Barber, J. *FEBS Lett.* **1982**, *140*, 165–168.
(9) Klimov, V. V.; Allakhverdiev, S. I.; Shuvalov, V. A.; Krasnovsky, A. A. *FEBS Lett.* **1982**, *148*, 307–312.
(10) Wydrzynski, T.; Sauer, K. *Biochim. Biophys. Acta* **1980**, *589*, 56–70.
(11) Kirby, J. A.; Robertson, A. S.; Smith, J. P.; Thompson, A. C.; Cooper, S. R.; Klein, M. P. *J. Am. Chem. Soc.* **1981**, *103*, 5529–5536.
(12) Kirby, J. A.; Gooding, D. B.; Wydrzynski, T.; Robertson, A. S.; Klein, M. P. *J. Am. Chem. Soc.* **1981**, *103*, 5537–5542.
(13) (a) Plaskin, P. M.; Stoufer, R. C.; Mathew, M.; Palenik, G. J. *J. Am. Chem. Soc.* **1972**, *94*, 2121–2122. (b) Dismukes, G. C.; Siderer, Y. *Proc. Natl. Acad. Sci. U.S.A.* **1981**, *78*, 274–278.
(14) Gersten, S. W.; Samuels, G. J.; Meyer, T. J. *J. Am. Chem. Soc.* **1982**, *104*, 4029–4030.

0002-7863/84/1506-2041$01.50/0

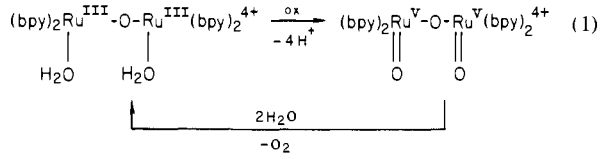

(1)

water molecules. During this process the ruthenium atoms cycle reversibly between d^5 and d^3 configurations; the same is probably true of the photosynthetic Mn centers. Essential features of the water oxidation process as described for the Ru dimer[3b] and suggested for the biological system[4] are initial conversion of coordinated water oxygen atoms to oxo ligands by sequential oxidation steps followed by oxygen–oxygen bond formation and O_2 displacement. These latter events likely occur with the reduction steps that restore the metal ions to their resting reduced state. Oxo ligands bonded to Mn(II) would be more subject to displacement as O_2 than bridging or terminal oxo ligands bonded to a more highly oxidized form of manganese.

In cases where localized metal and quinone electronic levels are close in energy, reversible electron transfer has been found to occur with great facility.[15] Quinone ligands have been used to direct charge at molybdenum and vanadium centers used as catalysts in an oxygen reduction system (eq 2).[16] The chemical

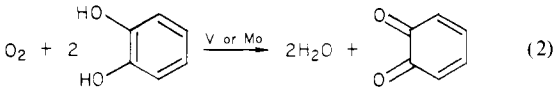

(2)

reaction associated with photosynthetic water oxidation is essentially the reverse process, driven photolytically, with a quinoid species, most likely a plastoquinone (PQ),[17] serving as the oxidizing agent (eq 3). A manganese–quinone complex could potentially

$$2H_2O + 4PQ \xrightarrow[\langle Mn^{2+},Mn^{2+}\rangle]{light} O_2 + 4PQ^{-}\cdot + 4H^{+} \qquad (3)$$

serve as a catalyst for this process, with changes in charge on the metal ion related to interconversion of isoelectronic bis(semiquinone)manganese(II) and bis(catecholato)manganese(IV) forms of the complex. In this report we present the synthesis of manganese complexes prepared with the 3,5-di-*tert*-butyl-1,2-benzoquinone ligand, characterization of the complexes, and the results of experiments that point to a manganese–quinone two-electron transfer reaction.[18]

Experimental Section

Compound Preparation. $Mn_4(O_2C_6H_2(t\text{-}Bu)_2)_8$. Procedure 1. Degassed solutions of $Mn_2(CO)_{10}$ (1.17 g, 3 mmol) in 40 mL of toluene and 3,5-di-*tert*-butyl-1,2-benzoquinone (2.64 g, 12 mmol) in 100 mL of toluene were combined under an atmosphere of dry N_2. The solution was irradiated with a sun lamp for 24 h. During irradiation the solution became dark green, and dark green crystals of $Mn_4(O_2C_6H_4(t\text{-}Bu)_2)_8$ formed. The crystals were separated from solution by filtration to give 1.81 g of the complex (61% yield).

Procedure 2. A solution containing 0.66 g (3.3 mmol) of $MnCl_2{\cdot}4H_2O$ in 85 mL of 95% ethanol was added dropwise to a solution consisting of 2.22 g (10 mmol) of 3,5-di-*tert*-butylcatechol and 1.12 g (20 mmol) of NaOH in 15 mL of degassed 95% ethanol. A white suspension formed immediately and the mixture was stirred in air for 1 h. During this time a green precipitate formed. The solution was evaporated to dryness and the solid obtained was dissolved in benzene. The benzene solution was filtered and the filtrate was extracted three times with 50% ethanol. Evaporation of the solvent gave the complex as a green powder. Recrystallization under an inert atmosphere first from heptane and then from toluene gave the dark green microcrystalline product. Anal. Calcd for $C_{112}H_{160}Mn_4O_{16}$: C, 67.86; H, 8.41; Mn, 11.09; O, 12.91. Found: C, 67.12; H, 8.08; Mn, 11.49.

Table I. Crystallographic Data for $Mn_4(O_2C_6H_2(t\text{-}Bu)_2)_8$

I^2W 1982.2	d(calcd) = 1.147 g cm^{-3}
triclinic	d(exptl) = 1.14 (1) g cm^{-3}
space group $P\bar{1}$	μ = 5.13 cm^{-1}
a = 14.822 (9) Å	Mo Kα ($\bar{\lambda}$ = 0.71069 Å)
b = 14.803 (4) Å	scan rate 2°/min
c = 16.428 (6) Å	angular range $3° \leq 2\theta \leq 45°$
α = 118.19 (2)°	scan range ±0.7°
β = 110.63 (3)°	data measured 5434
γ = 92.86 (4)°	data $F_o^2 > 3\sigma(F_o^2)$ 2756
V = 2869.2 Å^3	p = 0.04
Z = 1	

$Mn(O_2C_6H_4(t\text{-}Bu)_2)_2(NC_5H_5)_2{\cdot}2NC_5H_5$. A sample of the tetramer (1.0 g) was dissolved in pyridine (50 mL) under dry N_2 to give a purple solution. The solvent was evaporated slowly with a flow of N_2 to give purple crystals of $Mn(O_2C_6H_4(t\text{-}Bu)_2)_2(NC_5H_5)_2$ in quantitative yield. Elemental analyses and the structure determination indicated that the complex isolated by this procedure was the bis(pyridine) solvate.

Structure Determination of $Mn_4(O_2C_6H_4(t\text{-}Bu)_2)_8$. A dark green crystal of the complex was mounted and aligned on a Syntex $P\bar{1}$ automated diffractometer. Centered settings of 25 independent high-angle reflections indicated the triclinic crystal system of the reduced dimensions given in Table I. Intensities were measured for 5434 independent reflections within the angular range $3° \leq 2\theta \leq 45°$. Atom locations were obtained by MULTAN. Refinement, including fixed contributions for all hydrogen atoms, and other calculations were carried out by using programs and procedures referenced previously.[19] The tetramer has qualitatively the same structure as the $Co_4(3,5\text{-}DBSQ)_8$ tetramer, and the atom-numbering scheme used in this study is the same as that used in the Co structure determination.[20] Refinement of the molecule converged with $R_F = 0.059$ and $R_{wF} = 0.063$ for 2756 independent reflections with $I_o > 3\sigma(I_o)$. Table II contains the final positional and thermal parameters for all independent atoms of the molecule.

Structure Determination of $Mn(O_2C_6H_2(t\text{-}Bu)_2)_2(NC_5H_5){\cdot}2NC_5H_5$. A purple crystal of the complex obtained directly from pyridine solution was mounted and aligned on the diffractometer used in the previous determination. The settings of 25 reflections indicated monoclinic symmetry and gave the unit cell dimensions listed in Table III. Intensities were measured for 4367 reflections within the angular range $3° \leq 2\theta \leq 50°$. Phases obtained from a refinement with the manganese atom fixed at the origin of the unit cell, a crystallographic inversion center, were used to locate other atoms of the molecule. Refinement of the complete independent half of the molecule converged with $R_F = 0.049$ and $R_{wF} = 0.056$ for 2429 independent reflections with $I_o > 3\sigma(I_o)$. Table IV contains the final positional and thermal parameters for all independent atoms of the molecule.

Physical Measurements. Variable-temperature (4.2–286 K) magnetic susceptibility data were obtained with a Princeton Applied Research Model 150A vibrating-sample magnetometer. A calibrated GaAs diode was used to monitor the sample temperature in conjunction with a $CuSO_4{\cdot}5H_2O$ standard. The data were least-squares fit with an adapted version of the function minimization program STEPT.[21]

Electronic absorption measurements were made on a Cary 14 spectrophotometer. Solution-state spectra were obtained with airtight quartz cells, and solid-state spectra were obtained as KBr pellets. Variable-temperature studies between 30 and 300 K were obtained on solids by using a Cryogenic Technology Inc. "Spectrim" closed-cycle refrigerator, while solution spectra studied in the range 230–300 K were recorded either in a glass Dewar with a quartz window or in quartz cells using a gas-cooled sample holder. Temperatures were monitored by using an iron–constantan thermocouple.

Electron paramagnetic resonance measurements between 350 and 100 K were made with a Varian gas-flow cavity insert, while those at 77 K were made by employing a quartz Dewar.

Experimental Results

Structural Features of $Mn_4(3,5\text{-}DBSQ)_8$. The results of our crystallographic study on $Mn_4(O_2C_6H_2(t\text{-}Bu)_2)_8$ indicate that it has a centrosymmetric tetrameric structure. A stereoview showing the molecule is given in Figure 1. Outer *tert*-butyl methyl carbon atoms have been omitted from this view for clarity, but these

(15) Buchanan, R. M.; Pierpont, C. G. *J. Am. Chem. Soc.* **1980**, *102*, 4951–4957.
(16) Cass, M. E.; Greene, D. L.; Buchanan, R. M.; Pierpont, C. G. *J. Am. Chem. Soc.* **1983**, *105*, 2680–2686.
(17) Nugent, J. H. A.; Evans, M. C. W.; Diner, B. A. *Biochim. Biophys. Acta* **1982**, *682*, 106–114.
(18) Lynch, M. W.; Hendrickson, D. N.; Fitzgerald, B. J.; Pierpont, C. G. *J. Am. Chem. Soc.* **1981**, *103*, 3961–3963.
(19) Pierpont, C. G. *Inorg. Chem.* **1977**, *16*, 636–639.
(20) Buchanan, R. M.; Fitzgerald, B. J.; Pierpont, C. G. *Inorg. Chem.* **1979**, *18*, 3439–3444.
(21) Chandler, J. P. Program 66, Quantum Chemistry Program Exchange, Indiana University, Bloomington, IN.

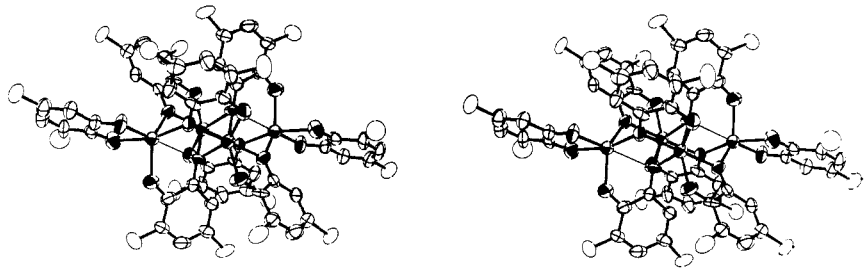

Figure 1. Stereoview showing the $Mn_4(3,5\text{-DBSQ})_8$ tetramer. Methyl carbon atoms of the *tert*-butyl substituents have been omitted.

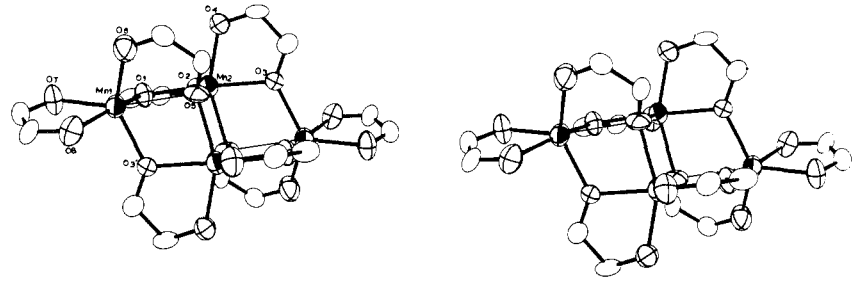

Figure 2. Stereoview showing the structure of the inner coordination sphere of the $Mn_4(3,5\text{-DBSQ})_8$ tetramer.

groups contribute to the solubility of this large complex molecule in nonpolar solvents. Structural features of the tetramer are similar to those of the cobalt and nickel analogues, where paramagnetic semiquinone ligands were found to be bonded to paramagnetic, divalent metal ions.[20] Bond lengths and angles of the tetramer are listed in Tables V and VI, and a stereoview showing the inner structure of the molecule is given in Figure 2. The two independent manganese ions have distorted octahedral coordination geometries with long Mn–O bond lengths. An average value of 2.138 (6) Å, calculated by excluding the anomalously long Mn–O(5) length, compares well with values found for complexes containing the high-spin Mn(II) ion listed in Table VII. Quinone ligands of the tetramer can be classified in three types. First, there are those that chelate with one metal ion and bridge to a second metal through one oxygen atom. Oxygen atoms that bond terminally generally have Mn–O lengths that are 0.1 Å shorter than those that bridge manganese ions. This class of ligands includes those with oxygen atoms 1 through 4 in Figure 2. The two ligands of the second type associated with oxygen atoms 5 and 6 chelate with Mn(1) but bridge to two adjacent metal ions through O(5). It is of interest that the Mn(1)–O(5) length within the chelate ring is the longest of the Mn–O(5) lengths, with a value of 2.526 (7) Å compared with values of 2.188 (8), and 2.212 (6) Å to Mn(2) and Mn(2)′. If the Mn–O(5) bond is ignored the remaining MnO_6 coordination polyhedron of Mn(1) shown in Figure 3 is quite close to a trigonal bipyramid, with O(3)′, O(6), and O(7) occupying equatorial sites and O(1) and O(8) in axial sites. Equatorial bond angles are 104.1 (3)°, 120.9 (2)°, and 132.0 (2)° and the axial O(1)–Mn(1)–O(8) angle is 163.3 (2)°. Oxygen O(5) then lies atop the O(1), O(3), O(6) face of this polyhedron, resulting in a capped trigonal-bipyramidal structure for the metal ion rather than an octahedron. The trans influence of the axial O(1)–Mn(1)–O(8) bonds is reflected in the significant difference between the Mn(1)–O(8) and Mn(1)–O(7) bond lengths. This

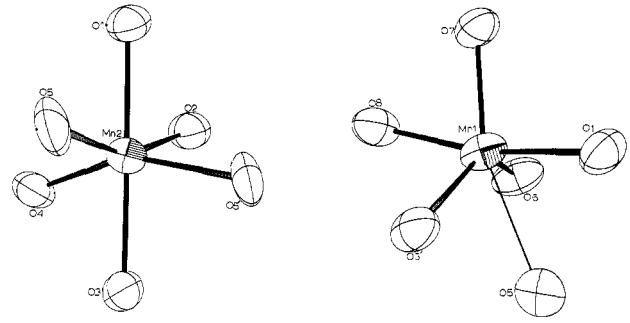

Figure 3. MnO_6 Coordination polyhedra of the two independent manganese ions of the $Mn_4(3,5\text{-DBSQ})_8$ tetramer.

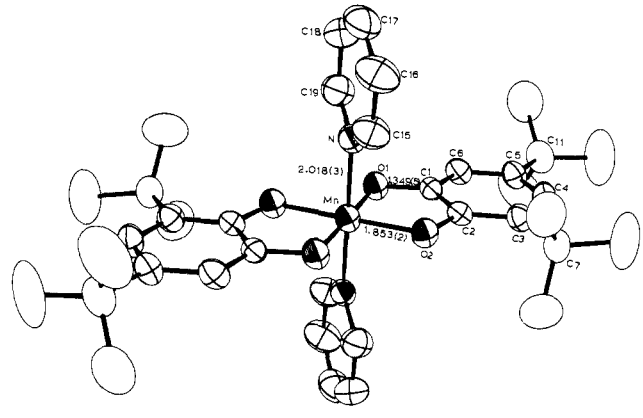

Figure 4. View of the $Mn(3,5\text{-DBCat})_2(py)_2$ molecule in the solid state at room temperature.

unique ligand is of the third type. It chelates with Mn(1) without an additional bridging interaction but shows a 0.1-Å difference in the Mn(1)–O(7) and Mn(1)–O(8) bond lengths, 2.078 (6) and 2.181 (10) Å, respectively. The MnO_6 coordination geometry of Mn(2) more closely resembles a regular octahedron, subject to the constrained bond angles of the chelating quinone ligands. Structural features of the cobalt analogue of this complex were found to be qualitatively similar, although the unusually long Mn(1)–O(5) length in the present structure is nearly 0.2 Å longer than the corresponding Co(1)–O(5) length, and the Co(1) coordination geometry more closely resembles an octahedron.[20]

As in other structure determinations on complexes containing quinone ligands, the C–O and carbonyl carbon C–C lengths have

(22) Stephens, F. S. *Acta Crystallogr., Sect. B.* **1977**, *B33*, 3492–3496.
(23) Hughes, B. B.; Haltiwanger, R. C.; Pierpont, C. G.; Hampton, M.; Blackmer, G. L. *Inorg. Chem.* **1980**, *19*, 1801–1803.
(24) Stults, B. R.; Marianelli, R. S.; Day, V. W. *Inorg. Chem.* **1975**, *14*, 722–730.
(25) Avdeef, A.; Costamagna, J. A.; Fackler, J. P. *Inorg. Chem.* **1974**, *13*, 1854–1863.
(26) Stein, J.; Fackler, J. P.; McClure, G. J.; Tee, J. A.; Chan, L. T. *Inorg. Chem.* **1979**, *18*, 3511–3519.
(27) Hartman, J. R.; Foxman, B. M.; Cooper, S. R. *J. Chem. Soc., Chem. Commun.* **1982**, 583–584.
(28) Camenzind, M. J.; Hollander, F. J.; Hill, C. L. *Inorg. Chem.* **1982**, *21*, 4301–4308.

Table II. Positional and Thermal Parameters for the Atoms of $Mn_4(O_2C_6H_2(t\text{-}Bu)_2)_8$

atom	x	y	z	B_{11}[a]	B_{22}	B_{33}	B_{12}	B_{13}	B_{23}
Mn(1)	0.17975 (11)	0.03132 (12)	−0.05334 (11)	3.30 (9)	4.00 (9)	3.80 (9)	0.40 (7)	1.70 (7)	1.30 (8)
Mn(2)	0.04514 (11)	−0.08435 (12)	0.03130 (11)	3.30 (9)	3.70 (9)	4.10 (9)	0.20 (7)	1.60 (3)	1.40 (8)
O(1)	0.1920 (4)	−0.0079 (4)	0.0629 (4)	3.8 (3)	4.8 (4)	3.9 (3)	0.4 (3)	1.8 (3)	2.5 (3)
O(2)	0.1352 (5)	−0.0569 (5)	0.1747 (5)	4.4 (3)	5.9 (4)	4.6 (4)	0.6 (3)	2.0 (3)	2.7 (3)
C(1)	0.2616 (7)	0.0150 (7)	0.1500 (7)	5.2 (7)	4.0 (6)	1.9 (6)	1.9 (5)	1.3 (6)	1.9 (5)
C(2)	0.2289 (7)	−0.0121 (7)	0.2112 (7)	3.9 (6)	4.1 (6)	3.1 (7)	1.2 (5)	1.7 (6)	1.2 (5)
C(3)	0.2990 (7)	0.0129 (8)	0.3092 (8)	4.2 (7)	6.8 (8)	4.7 (7)	1.2 (7)	2.2 (6)	4.0 (6)
C(4)	0.3946 (7)	0.0586 (8)	0.3388 (8)	3.8 (7)	7.9 (8)	4.9 (7)	1.5 (6)	1.9 (6)	3.9 (6)
C(5)	0.4292 (7)	0.0860 (8)	0.2809 (8)	4.0 (7)	5.0 (7)	4.2 (7)	1.6 (5)	1.2 (6)	2.1 (6)
C(6)	0.3623 (7)	0.0646 (8)	0.1876 (8)	2.8 (6)	5.3 (7)	5.3 (7)	0.2 (5)	1.2 (5)	3.3 (6)
C(7)	0.2681 (8)	−0.0148 (10)	0.3743 (9)	4.6 (7)	10.2 (10)	7.1 (8)	1.6 (7)	2.5 (7)	6.3 (8)
C(8)	0.1845 (9)	0.0337 (11)	0.3939 (9)	7.6 (8)	14.2 (12)	6.2 (8)	1.0 (8)	3.8 (7)	5.4 (8)
C(9)	0.2277 (11)	−0.1348 (13)	0.3191 (12)	13.0 (12)	13.6 (14)	15.8 (14)	2.2 (11)	5.9 (11)	11.9 (13)
C(10)	0.3500 (9)	0.0209 (15)	0.4771 (10)	6.8 (9)	30.2 (20)	9.9 (10)	3.3 (11)	2.7 (8)	16.2 (13)
C(11)	0.5398 (7)	0.1359 (8)	0.3193 (8)	3.5 (6)	6.7 (8)	4.3 (7)	1.1 (6)	0.7 (5)	3.4 (7)
C(12)	0.5830 (9)	0.2201 (10)	0.4293 (10)	6.0 (8)	9.4 (10)	7.4 (9)	−1.7 (7)	0.8 (7)	1.4 (8)
C(13)	0.5932 (9)	0.0493 (11)	0.3089 (11)	4.2 (7)	9.0 (10)	12.8 (12)	1.2 (7)	2.3 (7)	3.3 (9)
C(14)	0.5581 (8)	0.1820 (15)	0.2632 (12)	2.6 (7)	32.1 (22)	17.6 (14)	−5.1 (9)	−2.4 (7)	21.1 (16)
O(3)	0.1092 (4)	0.1493 (4)	0.0120 (4)	3.7 (3)	2.7 (3)	5.3 (4)	0.5 (3)	2.5 (3)	1.2 (3)
O(4)	−0.0255 (4)	0.2473 (5)	0.0505 (5)	3.3 (3)	3.7 (4)	5.4 (4)	0.3 (3)	1.4 (3)	1.0 (3)
C(15)	0.1352 (7)	0.2519 (8)	0.0597 (7)	4.5 (7)	4.0 (6)	3.2 (6)	1.5 (6)	2.5 (5)	2.1 (5)
C(16)	0.0602 (7)	0.3071 (7)	0.0826 (6)	4.2 (6)	2.3 (6)	1.8 (5)	1.1 (5)	0.8 (5)	−0.2 (4)
C(17)	0.0842 (7)	0.4198 (8)	0.1373 (7)	4.2 (6)	3.8 (7)	4.8 (6)	1.2 (5)	2.4 (5)	1.7 (6)
C(18)	0.1807 (8)	0.4718 (7)	0.1695 (8)	4.7 (7)	3.5 (6)	6.2 (7)	1.0 (6)	2.5 (6)	1.5 (5)
C(19)	0.2580 (7)	0.4231 (8)	0.1518 (7)	4.8 (7)	3.9 (7)	4.2 (6)	0.3 (6)	2.0 (5)	1.9 (5)
C(20)	0.2340 (7)	0.3129 (8)	0.0971 (7)	2.9 (5)	4.5 (7)	4.2 (6)	0.7 (5)	2.2 (5)	1.9 (5)
C(21)	0.0079 (8)	0.4778 (8)	0.1609 (9)	4.9 (7)	3.9 (7)	8.4 (9)	1.1 (6)	3.3 (7)	1.9 (7)
C(22)	0.0511 (9)	0.5994 (9)	0.2255 (12)	5.5 (7)	4.2 (8)	19.0 (13)	2.7 (6)	5.8 (8)	2.8 (8)
C(23)	−0.0806 (8)	0.4496 (10)	0.0622 (10)	3.9 (7)	8.4 (9)	11.7 (10)	1.6 (6)	2.1 (7)	5.9 (8)
C(24)	−0.0284 (9)	0.4474 (9)	0.2217 (9)	6.3 (8)	7.0 (9)	8.3 (8)	1.3 (6)	3.9 (7)	1.0 (7)
C(25)	0.3613 (7)	0.4894 (8)	0.1907 (8)	3.2 (6)	4.4 (7)	6.7 (7)	−0.6 (6)	2.4 (6)	1.9 (6)
C(26)	0.3980 (9)	0.5782 (10)	0.2995 (10)	4.8 (7)	8.3 (10)	9.7 (10)	−2.2 (7)	1.2 (7)	−1.5 (8)
C(27)	0.4378 (9)	0.4292 (10)	0.1894 (12)	3.5 (7)	6.3 (9)	17.8 (14)	−0.8 (7)	3.8 (8)	2.2 (9)
C(28)	0.3587 (10)	0.5365 (16)	0.1300 (14)	6.9 (9)	28.6 (20)	20.9 (17)	−7.0 (10)	−1.2 (9)	20.4 (17)
O(5)	0.0065 (4)	−0.0602 (4)	−0.0971 (4)	4.8 (4)	2.6 (3)	2.9 (3)	0.6 (3)	1.4 (3)	−0.2 (3)
O(6)	0.1269 (5)	−0.1121 (5)	−0.1900 (5)	4.6 (4)	5.3 (4)	4.9 (4)	−0.3 (3)	2.4 (3)	0.7 (3)
C(29)	−0.0285 (7)	−0.1387 (7)	−0.1903 (7)	2.4 (5)	4.1 (4)	4.0 (6)	0.3 (5)	1.6 (5)	1.2 (5)
C(30)	0.0349 (7)	−0.1679 (7)	−0.2431 (8)	4.2 (6)	3.1 (6)	5.0 (7)	0.2 (5)	2.1 (6)	0.9 (6)
C(31)	−0.0010 (8)	−0.2489 (8)	−0.3499 (7)	5.8 (7)	4.8 (6)	3.7 (6)	−0.1 (6)	2.9 (6)	0.2 (5)
C(32)	−0.0987 (8)	−0.3075 (8)	−0.3967 (8)	5.8 (7)	4.3 (8)	4.5 (7)	−0.2 (6)	2.3 (6)	−0.2 (5)
C(33)	−0.1635 (7)	−0.2866 (7)	−0.3478 (7)	4.5 (6)	4.3 (7)	2.7 (6)	0.8 (5)	1.1 (5)	1.2 (5)
C(34)	−0.1288 (7)	−0.2040 (7)	−0.2475 (7)	3.5 (6)	4.0 (6)	3.3 (6)	0.9 (5)	1.5 (5)	1.6 (5)
C(35)	0.0645 (9)	−0.2707 (10)	−0.4053 (9)	6.2 (8)	8.8 (6)	5.4 (8)	0.7 (7)	4.1 (7)	0.7 (7)
C(36)	0.1526 (10)	−0.3039 (11)	−0.3558 (11)	5.5 (8)	11.3 (12)	11.3 (11)	0.1 (8)	5.6 (8)	−0.6 (9)
C(37)	0.0115 (10)	−0.3564 (12)	−0.5172 (9)	9.3 (9)	13.7 (12)	5.7 (8)	−3.4 (9)	5.6 (7)	−3.1 (8)
C(38)	0.1055 (11)	−0.1691 (11)	−0.3977 (10)	11.9 (11)	11.9 (11)	8.6 (9)	−1.6 (9)	7.1 (8)	3.4 (9)
C(39)	−0.2699 (7)	−0.3600 (8)	−0.4122 (8)	3.5 (6)	3.9 (7)	4.7 (7)	−0.7 (5)	0.2 (6)	0.6 (6)
C(40)	−0.3328 (8)	−0.3312 (9)	−0.3538 (9)	4.2 (6)	6.8 (8)	8.5 (8)	−0.2 (6)	2.7 (6)	0.9 (7)
C(41)	−0.3197 (9)	−0.3568 (13)	−0.5071 (10)	6.0 (8)	19.1 (15)	6.6 (9)	−3.1 (9)	−2.5 (7)	7.4 (10)
C(42)	−0.2633 (8)	−0.4705 (9)	−0.4395 (10)	4.8 (7)	5.4 (8)	10.9 (10)	−1.1 (6)	2.7 (7)	0.3 (7)
O(7)	0.3334 (4)	0.0679 (5)	−0.0063 (5)	3.5 (4)	6.6 (5)	6.0 (4)	0.4 (3)	2.0 (3)	4.2 (4)
O(8)	0.2039 (5)	0.1093 (5)	−0.1309 (5)	4.0 (4)	6.8 (4)	5.4 (4)	1.9 (3)	2.2 (3)	3.5 (4)
C(43)	0.3670 (7)	0.1190 (7)	−0.0393 (7)	3.5 (7)	4.0 (6)	4.6 (7)	0.4 (5)	2.4 (6)	1.9 (5)
C(44)	0.2948 (7)	0.1432 (7)	−0.1088 (7)	2.8 (6)	4.7 (7)	3.4 (6)	1.1 (5)	2.0 (6)	1.3 (5)
C(45)	0.3306 (8)	0.2023 (8)	−0.1450 (8)	4.5 (7)	5.6 (7)	6.2 (7)	1.2 (6)	3.6 (6)	3.7 (6)
C(46)	0.4311 (8)	0.2349 (7)	−0.1089 (9)	6.9 (8)	3.6 (6)	9.0 (9)	2.4 (6)	5.4 (7)	4.5 (6)
C(47)	0.5033 (8)	0.2136 (7)	−0.0401 (8)	5.1 (7)	3.8 (6)	6.8 (8)	1.4 (6)	3.3 (6)	3.3 (6)
C(48)	0.4698 (7)	0.1547 (8)	−0.0084 (7)	3.3 (6)	4.8 (6)	5.1 (6)	1.0 (5)	1.6 (5)	3.4 (5)
C(49)	0.2568 (9)	0.2249 (9)	−0.2218 (9)	7.3 (8)	6.4 (9)	6.8 (8)	2.9 (7)	2.2 (7)	4.9 (8)
C(50)	0.1935 (10)	0.2897 (11)	−0.1763 (10)	11.1 (10)	10.2 (11)	10.3 (10)	7.9 (9)	5.1 (9)	6.1 (9)
C(51)	0.3067 (10)	0.2844 (12)	−0.2534 (11)	11.6 (11)	14.4 (12)	14.1 (12)	4.5 (9)	6.0 (9)	13.0 (11)
C(52)	0.1919 (10)	0.1207 (11)	−0.3159 (10)	10.1 (9)	9.5 (11)	6.9 (8)	3.3 (9)	2.1 (7)	4.9 (8)
C(53)	0.6132 (8)	0.2587 (8)	−0.0053 (9)	4.7 (7)	5.0 (8)	8.3 (9)	0.1 (6)	3.7 (7)	2.3 (7)
C(54)	0.6785 (8)	0.2189 (11)	0.0575 (11)	2.6 (6)	14.1 (12)	15.0 (12)	0.0 (7)	2.1 (7)	9.7 (11)
C(55)	0.6379 (8)	0.2250 (9)	−0.0967 (9)	5.0 (7)	8.4 (9)	10.5 (9)	1.8 (6)	4.4 (7)	5.1 (8)
C(56)	0.6372 (9)	0.3767 (9)	0.0577 (9)	6.5 (8)	5.7 (8)	9.0 (9)	−1.1 (6)	3.4 (7)	1.0 (7)

[a] The form of the anisotropic thermal ellipsoid is $\exp[-0.25(B_{11}h^2a^{*2} + B_{22}k^2b^{*2} + B_{33}l^2c^{*2} + 2B_{12}hka^*b^* + 2B_{13}hla^*c^* + 2B_{23}klb^*c^*)]$. The quantities given in the table are in units of Å^2.

values characteristic of ligand charge. These values are 1.289 (12) Å for the C–O lengths and 1.455 (17) Å for the associated C–C bonds, values consistent with semiquinone coordination for the ligands.[29] Structural features of the complex, therefore, indicate divalent metal ions bonded by paramagnetic semiquinone ligands, $Mn_4(3,5\text{-}DBSQ)_8$, in a tetrameric unit.

Structural Features of Mn(3,5-DBCat)$_2$(py)$_2$. Crystals of the pyridine addition product of $Mn_4(3,5\text{-}DBSQ)_8$ obtained from pyridine solution in the form of a solvate $Mn(O_2C_6H_2(t\text{-}Bu)_2)_2(NC_5H_5)_2 \cdot 2NC_5H_5$ were found to contain monomeric complex units located about crystallographic inversion centers. A view of

(29) Pierpont, C. G.; Buchanan, R. M. *Coord. Chem. Rev.* **1981**, *38*, 45–87.

Table III. Crystallographic Data for $Mn[O_2C_6H_2(t\text{-}Bu)_2]_2[NC_5H_5]_2 \cdot 2NC_5H_5$

I^2W 812.02	d(calcd), g cm^{-3} 1.198
monoclinic	d(exptl), g cm^{-3} 1.21 (1)
space group $P2_1/c$	μ = 3.58 cm^{-1}
a = 9.032 (4) Å	Mo Kα (λ = 0.71069 Å)
b = 18.862 (9) Å	scan rate 2°/min
c = 13.296 (7) Å	angular range $3° \leq 2\theta \leq 50°$
β = 96.59 (4)°	scan range ±0.7°
V = 2250.3 Å^3	data measured 4367
Z = 2	data $F_o > 3\sigma(F_o^2)$ 2429
	P = 0.04

the complex molecule is shown in Figure 4; bond lengths and angles for the molecule are given in Table VIII. Features of the MnO_4N_2 coordination polyhedron resemble a regular octahedron but with significant structural differences from the MnO_6 units of the tetramer. Independent Mn–O lengths of 1.854 (2) Å are more than 0.2 Å shorter than values found for the tetramer but compare well with values reported for d^3 Mn(IV) complexes listed in Table VII. In particular, Mn–O and Mn–N lengths compare quite favorably with values reported for $Mn(TPP)(OCH_3)_2$ and $Mn(3,5\text{-}DBCat)_3^{2-}$ but differ significantly from the values of $Mn(acac)_2(phen)$ containing Mn(II) and $[Mn(acac)_2N_3]_n$ with Mn(III). As before, the quinone C–O and C–C bond lengths are sensitive to the charge distribution in the complex. In this molecule the average C–O length of 1.349 (4) Å and a C(1)–C(2) length of 1.402 (4) Å indicate that the ligands are chelated in the fully reduced catecholate form. Structural features of this molecule indicate a complex of Mn(IV), $Mn(3,5\text{-}DBCat)_2(py)_2$.

Electronic Spectra. Electronic absorption spectra recorded on $Mn_4(3,5\text{-}DBSQ)_8$ in toluene solution and in the solid state closely resemble the spectra of related Co and Ni tetramers, which are also dark green. Two transitions are observed in all three cases in the region between 350 and 900 nm, with values listed in Table IX. Similar spectra are obtained in the solid state but with slight asymmetry in the low-energy absorptions.

The electronic absorption spectrum of $Mn(3,5\text{-}DBCat)_2(py)_2$ shows an interesting temperature dependence. Crystals of the complex, which are dark purple, give a green solution in toluene at room temperature. When the toluene solution is cooled to temperatures below 250 K, it turns to the intense purple color of the complex in the solid state. Similar behavior was observed in pyridine solution, although the green/purple transition temperature is about 350 K in this solvent. Electronic spectra were recorded for the complex in both toluene and pyridine solutions. Solid-state spectra could not be obtained due to decomposition in the KBr matrix. The observed electronic transitions are listed in Table IX and the temperature dependence of the toluene solution is shown in Figure 5. In toluene at 299 K the low-energy region of the spectrum consists of a single absorption at 780 nm, which is quite similar to the spectra observed for the green tetramers of Co, Ni, and Mn, which all show a broad transition in the region between 755 and 780 nm. It also resembles the spectra of $Ni(3,5\text{-}DBSQ)_2(bpy)$ and $Co(3,5\text{-}DBSQ)_2(bpy)$, which have ab-

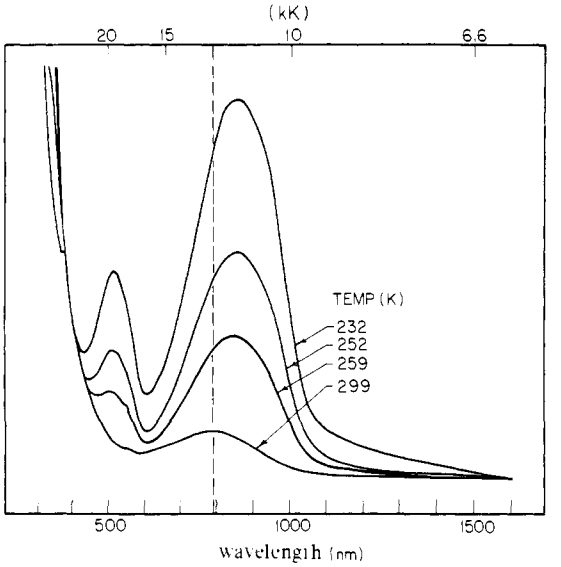

Figure 5. Optical spectra recorded on the pyridine addition product in toluene solution showing the transition from $Mn^{IV}(3,5\text{-}DBCat)_2(py)_2$ at 232 K to $Mn^{II}(3,5\text{-}DBSQ)_2(py)_2$ at 299 K.

Table IV. Positional and Thermal Parameters for the Atoms of $Mn[O_2C_6H_2(t\text{-}Bu)_2]_2[NC_5H_5]_2 \cdot 2NC_5H_5$

atom	x	y	z	B_{11}[a]	B_{22}	B_{33}	B_{12}	B_{13}	B_{23}
Mn	0	0	0	3.76 (3)	2.70 (3)	2.67 (3)	0.17 (3)	0.46 (2)	−0.06 (3)
O(1)	−0.05714 (23)	0.09435 (11)	0.00217 (15)	4.41 (11)	2.81 (1)	2.86 (10)	0.10 (8)	0.23 (9)	−0.16 (8)
O(2)	−0.08106 (23)	−0.00047 (12)	−0.13448 (14)	4.38 (11)	2.81 (9)	2.89 (9)	0.11 (10)	0.27 (8)	−0.29 (9)
C(1)	−0.1274 (3)	0.11502 (16)	−0.08811 (22)	3.12 (16)	2.72 (15)	2.48 (14)	−0.42 (12)	0.30 (12)	0.18 (12)
C(2)	−0.1379 (3)	0.06324 (16)	−0.16421 (23)	3.04 (16)	2.55 (15)	2.75 (14)	−0.13 (12)	0.67 (12)	0.21 (12)
C(3)	−0.2053 (4)	0.07908 (18)	−0.26095 (24)	3.70 (17)	3.39 (16)	2.70 (15)	0.01 (14)	0.64 (12)	−0.01 (12)
C(4)	−0.2616 (4)	0.14745 (19)	−0.27609 (25)	4.71 (20)	3.80 (17)	2.81 (16)	0.28 (15)	0.03 (13)	0.38 (13)
C(5)	−0.2545 (4)	0.19919 (18)	−0.20115 (26)	4.35 (19)	3.07 (16)	3.37 (16)	0.26 (14)	0.50 (14)	0.67 (13)
C(6)	−0.1853 (4)	0.18148 (17)	−0.10603 (24)	4.37 (18)	2.50 (15)	3.12 (16)	−0.04 (13)	0.81 (13)	−0.24 (12)
C(7)	−0.2151 (4)	0.02370 (18)	−0.34602 (25)	4.86 (20)	3.99 (18)	2.56 (15)	0.14 (15)	0.25 (14)	−0.34 (12)
C(8)	−0.0640 (5)	−0.00517 (25)	−0.3598 (3)	6.53 (24)	7.46 (26)	4.46 (19)	0.71 (23)	1.56 (17)	−2.09 (20)
C(9)	−0.3147 (6)	−0.03672 (26)	−0.3204 (3)	9.0 (3)	6.63 (26)	5.42 (24)	−3.15 (24)	2.09 (22)	−2.64 (20)
C(10)	−0.2796 (7)	0.05428 (25)	−0.4473 (3)	13.7 (4)	6.72 (28)	3.44 (20)	2.46 (28)	−1.65 (24)	−1.29 (20)
C(11)	−0.3203 (5)	0.27324 (20)	−0.2187 (3)	6.4 (3)	3.29 (18)	4.66 (20)	0.80 (17)	0.13 (18)	0.68 (15)
C(12)	−0.2024 (6)	0.32972 (23)	−0.1878 (4)	11.5 (4)	3.30 (20)	8.02 (31)	0.57 (23)	−0.61 (27)	0.49 (20)
C(13)	−0.4439 (7)	0.28259 (27)	−0.1518 (4)	10.1 (4)	6.43 (29)	12.42 (36)	4.83 (27)	4.46 (25)	3.27 (28)
C(14)	−0.3753 (8)	0.28725 (25)	−0.3287 (4)	17.6 (5)	4.42 (24)	6.53 (28)	3.85 (28)	−3.18 (27)	0.85 (21)
N(1)	0.1984 (3)	0.02841 (14)	−0.0436 (2)	3.7 (1)	3.10 (12)	2.90 (13)	−0.11 (11)	0.42 (11)	0.12 (10)
C(15)	0.2584 (4)	−0.00869 (21)	−0.1138 (3)	4.7 (2)	4.44 (20)	5.03 (20)	−0.06 (17)	1.76 (16)	−0.16 (17)
C(16)	0.3893 (5)	0.00900 (25)	−0.1472 (3)	5.6 (2)	5.99 (25)	6.44 (25)	0.00 (22)	2.91 (19)	0.22 (21)
C(17)	0.4645 (5)	0.06701 (28)	−0.1084 (4)	4.2 (2)	7.63 (30)	6.09 (25)	−0.19 (21)	1.58 (19)	2.23 (23)
C(18)	0.4050 (5)	0.10558 (24)	−0.0364 (3)	5.2 (2)	5.95 (25)	5.94 (24)	−2.14 (20)	0.04 (20)	0.48 (20)
C(19)	0.2725 (5)	0.08454 (21)	−0.0048 (3)	5.2 (2)	4.55 (20)	4.07 (19)	−0.81 (18)	0.91 (16)	−0.44 (16)
C(20)	0.272 (1)	0.137 (1)	−0.363 (1)	13.5 (8)	6.8 (5)	13.5 (8)	1.4 (5)	0.9 (6)	1.5 (5)
C(21)	0.192 (1)	0.157 (1)	−0.296 (1)	9.7 (6)	11.7 (7)	11.3 (7)	0.3 (5)	2.0 (5)	2.5 (5)
C(22)	0.116 (1)	0.212 (1)	−0.308 (1)	7.2 (5)	13.9 (8)	19.5 (11)	3.4 (5)	4.3 (5)	3.2 (7)
C(23)	0.110 (1)	0.249 (1)	−0.393 (1)	13.4 (9)	12.8 (7)	17.1 (11)	3.7 (6)	−0.7 (7)	8.5 (8)
C(24)	0.193 (2)	0.220 (1)	−0.470 (1)	16.6 (18)	21.8 (19)	11.2 (9)	−4.1 (13)	0.1 (10)	6.2 (12)
C(25)	0.284 (1)	0.164 (1)	−0.446 (1)	17.5 (10)	12.7 (8)	8.3 (6)	−1.9 (7)	1.1 (6)	−0.5 (5)

[a] The form of the anisotropic thermal ellipsoid is $\exp[-0.25(B_{11}h^2a^{*2} + B_{22}k^2b^{*2} + B_{33}l^2c^{*2} + 2B_{12}hka^*b^* + 2B_{13}hla^*c^* + 2B_{23}klb^*c^*)]$. The quantities given in the table are in units of Å^2.

Table V. Bond Lengths (Å) for $Mn_4[O_2C_6H_2(t\text{-}Bu)_2]_8$

Manganese-Oxygen Bond Lengths			
Mn(1)-O(1)	2.197 (9)	Mn(2)-O(1)	2.166 (7)
Mn(1)-O(3)	2.133 (7)	Mn(2)-O(2)	2.078 (7)
Mn(1)-O(5)	2.526 (7)	Mn(2)-O(3)′	2.165 (7)
Mn(1)-O(6)	2.062 (5)	Mn(2)-O(4)′	2.074 (6)
Mn(1)-O(7)	2.078 (6)	Mn(2)-O(5)	2.188 (8)
Mn(1)-O(8)	2.181 (8)	Mn(2)-O(5)′	2.212 (6)
Nonbonding Mn-Mn Separations			
Mn(1)-Mn(1)′	6.321 (5)	Mn(1)-Mn(2)′	3.564 (3)
Mn(1)-Mn(2)	3.565 (3)	Mn(2)-Mn(2)′	3.298 (4)
Ligand 1			
O(1)-C(1)	1.302 (11)	C(3)-C(4)	1.345 (15)
O(2)-C(2)	1.294 (12)	C(4)-C(5)	1.422 (21)
C(1)-C(2)	1.453 (19)	C(5)-C(6)	1.368 (15)
C(2)-C(3)	1.424 (15)	C(1)-C(6)	1.399 (14)
Ligand 2			
O(3)-C(15)	1.292 (11)	C(17)-C(18)	1.375 (15)
O(4)-C(16)	1.295 (12)	C(18)-C(19)	1.427 (17)
C(15)-C(16)	1.462 (15)	C(19)-C(20)	1.389 (14)
C(16)-C(17)	1.421 (13)	C(15)-C(20)	1.431 (14)
Ligand 3			
O(5)-C(29)	1.290 (9)	C(31)-C(32)	1.378 (15)
O(6)-C(30)	1.293 (11)	C(32)-C(33)	1.416 (19)
C(29)-C(30)	1.443 (17)	C(33)-C(34)	1.383 (11)
C(30)-C(31)	1.445 (13)	C(29)-C(34)	1.429 (12)
Ligand 4			
O(7)-C(43)	1.287 (17)	C(45)-C(46)	1.356 (16)
O(8)-C(44)	1.271 (13)	C(46)-C(47)	1.428 (18)
C(43)-C(44)	1.463 (16)	C(47)-C(48)	1.360 (20)
C(44)-C(45)	1.437 (20)	C(43)-C(48)	1.407 (14)

Table VI. Selected Bond Angles (deg) for $Mn_4[O_2C_6H_2(t\text{-}Bu)_2]_8$

Angles about Mn(1)			
O(1)-Mn(1)-O(3)	88.9 (3)	O(3)-Mn(1)-O(8)	87.2 (3)
O(1)-Mn(1)-O(5)	72.3 (2)	O(5)-Mn(1)-O(6)	69.9 (3)
O(1)-Mn(1)-O(6)	105.7 (3)	O(5)-Mn(1)-O(7)	160.9 (3)
O(1)-Mn(1)-O(7)	92.8 (3)	O(5)-Mn(1)-O(8)	121.5 (2)
O(1)-Mn(1)-O(8)	163.3 (2)	O(6)-Mn(1)-O(7)	104.1 (3)
O(3)-Mn(1)-O(5)	71.8 (2)	O(6)-Mn(1)-O(8)	88.9 (3)
O(3)-Mn(1)-O(6)	132.0 (2)	O(7)-Mn(1)-O(8)	75.4 (3)
O(3)-Mn(1)-O(7)	120.9 (2)		
Angles about Mn(2)			
O(1)-Mn(2)-O(2)	76.4 (3)	O(2)-Mn(2)-O(5)′	92.4 (3)
O(1)-Mn(2)-O(3)	172.4 (3)	O(3)′-Mn(2)-O(4)′	76.2 (3)
O(1)-Mn(2)-O(4)'	108.0 (3)	O(3)′-Mn(2)-O(5)	93.2 (3)
O(1)-Mn(2)-O(5)	80.0 (3)	O(3)′-Mn(2)-O(5)′	77.6 (2)
O(1)-Mn(2)-O(5)′	98.0 (2)	O(4)'-Mn(2)-O(5)	97.5 (3)
O(2)-Mn(2)-O(3)'	109.7 (3)	O(4)′-Mn(2)-O(5)′	153.7 (3)
O(2)-Mn(2)-O(4)′	97.4 (3)	O(5)-Mn(2)-O(5)′	82.9 (3)
O(2)-Mn(2)-O(5)	155.1 (3)		
Ligand 1			
Mn(1)-O(1)-C(1)	135.8 (7)	O(1)-C(1)-C(6)	124.8 (12)
Mn(2)-O(2)-C(1)	113.9 (8)	O(2)-C(2)-C(1)	118.0 (9)
Mn(2)-O(2)-C(2)	116.0 (8)	O(2)-C(2)-C(3)	122.0 (12)
O(1)-C(1)-C(2)	115.7 (9)		
Ligand 2			
Mn(1)-O(3)-C(15)	133.6 (7)	O(3)-C(15)-C(20)	123.3 (9)
Mn(2)-O(3)-C(15)	143.5 (7)	O(4)-C(16)-C(15)	115.7 (8)
Mn(2)-O(4)-C(16)	104.7 (6)	O(4)-C(16)-C(17)	124.0 (10)
O(3)-C(15)-C(16)	117.4 (9)		
Ligand 3			
Mn(1)-O(5)-C(29)	106.6 (7)	O(5)-C(29)-C(30)	120.6 (8)
Mn(2)-O(5)-C(29)	121.9 (7)	O(5)-C(29)-C(34)	124.1 (10)
Mn(2)′-O(5)-C(29)	129.1 (7)	O(6)-C(30)-C(29)	115.5 (8)
Mn(1)-O(6)-C(30)	125.1 (7)	O(6)-C(30)-C(31)	120.8 (11)
Ligand 4			
Mn(1)-O(7)-C(43)	116.4 (6)	O(7)-C(43)-C(48)	122.3 (10)
Mn(1)-O(8)-C(44)	115.1 (7)	O(8)-C(44)-C(43)	115.0 (12)
O(7)-C(43)-C(44)	118.1 (9)	O(8)-C(44)-C(45)	125.9 (10)

sorptions at 765 and 770 nm, respectively.[15,30] As the temperature of the solution is decreased to 232 K, the low-energy transition moves to 824 nm and increases markedly in intensity, and a new transition at 515 nm appears. This change is shown in Figure 5. Since a solid-state spectrum could not be obtained for the complex, we cannot verify that this spectrum is that of the complex characterized crystallographically; however, magnetic resonance experiments described in the following section strongly suggest that this is the spectrum of $Mn(3,5\text{-}DBCat)_2(py)_2$. We have further established that this temperature dependence is reversible by cooling and warming the toluene solution through several thermal cycles.

Magnetism and EPR Spectra. Solid samples of the $Mn_4(3,5\text{-}DBSQ)_8$ tetramer have a magnetic moment of 5.1 μ_B per $Mn(3,5\text{-}DBSQ)_2$ unit at room temperature. This value indicates weak spin–spin coupling involving both paramagnetic semiquinone ligands and the high-spin Mn(II) centers, coupling of the type found for the Ni and Co tetramers, which have moments of 4.35 and 4.58 μ_B per monomeric unit at room temperature. Attempts were made to resolve the EPR spectrum of $Mn_4(3,5\text{-}DBSQ)_8$ in toluene solution at 300 and 100 K and in the solid state at 100 K, but no spectrum was observed.

The magnetic moment of $Mn(3,5\text{-}DBCat)_2(py)_2$ in the solid state was found to be 4.2 μ_B at room temperature. This value remains nearly constant within the temperature range 286–30 K but drops to 3.9 μ_B between 20 and 4.2 K. Complexes of Mn(IV) commonly have magnetic moments of 3.9 μ_B, and the slight temperature dependence is likely related to a moderate zero-field splitting contribution. EPR spectra were recorded for $Mn(3,5\text{-}DBCat)_2(py)_2$ in toluene and pyridine solutions over the temperature range 300–100 K and for the solid complex over the range 300–4.2 K. As the temperatures of the toluene solution was increased from 230 K the intensity of the EPR spectrum decreased until at approximately 260 K no spectrum could be resolved. This corresponds to the temperature range over which thermochromic behavior and the associated change in the electronic spectrum shown in Figure 5 were found to occur. EPR spectra recorded in the three media are shown in Figure 6 and all have the same general appearance of spectra associated with rhombically distorted octahedral d^3 metal ion complexes. Computer simulation would be required for quantitative determination of the spectral parameters g, D, and E. However, from Hempel and co-workers' analysis of the spectra obtained for *trans*-$Cr(en)_2A_2^{n+}$, A = SCN^-, Cl^-, H_2O, and OH^-, which are also rhombically distorted d^3 complexes, estimates of the zero-field splitting tensor D and the E/D ratio can be obtained.[31] The value of D is in the 0.4–0.5-cm^{-1} range and, although the estimate of E/D is quite sensitive to the exact spectral energy, it appears that $E/D \leq 0.1$.

In toluene solution at a temperature of 180 K, ^{55}Mn ($I = {}^5/_2$) hyperfine coupling can be observed on one resonance. The average value for this interaction is 61 ± 4 G (57 × 10^{-4} cm^{-1}), which is closer to values observed for Mn(IV) than for Mn(II). In a MgO matrix Mn(IV) hyperfine coupling of 77 G (72 × 10^{-4} cm^{-1}) has been reported while for Mn(II) the value is 87 G (81 × 10^{-4} cm^{-1}).[32]

Discussion

Charge Distribution in Manganese–Quinone Complexes. A unique and particarly interesting feature of the metal–quinone complexes is that metal and quinone electronic levels remain discrete in a molecular orbital sense and yet are quite close in energy. As a consequence, the electronic structure of a metal

(30) Lynch, M. W.; Buchanan, R. M.; Pierpont, C. G.; Hendrickson, D. N. *Inorg. Chem.* **1981**, *20*, 1038–1046.

(31) Hempel, J. C.; Morgan, L. O.; Lewis, W. B. *Inorg. Chem.* **1970**, *9*, 2064–2072.

(32) (a) McGarvey, B. R. In "Transition Metal Chemistry"; Carlin, R. L., Ed.; Marcel Dekker: New York, 1966; Vol. 3, p 89. (b) Nakadu, M.; Awazu, K.; Ibuki, S.; Miyako, T.; Date, M. *J. Phys. Soc. Jpn.* **1964**, *19*, 781–786.

Table VII. Representative Mn-O and Mn-N Bond Lengths

complex	Mn oxidation state	Mn-O, Å	Mn-N, Å	ref
$Mn_4(3,5\text{-DBSQ})_8$	II	2.062 (5)-2.526 (7)		this work
$Mn(12\text{-Crown-4})_2^{2+}$	II	2.24 (2)-2.37 (2)		23
$Mn(acac)_2(phen)$	II	2.116 (5)-2.152 (5)	2.307 (5)	22
$Mn(trop)_3$	III	2.001		25
$Mn(EDTA)^-$	III	1.898 (11)-2.036 (12)	2.223 (14)	26
$[Mn(acac)_2(N_3)]_n$	III	1.910 (1)	2.245 (2)	24
$Mn(3,5\text{-DBCat})_2(py)_2$	IV	1.854 (2)	2.018 (3)	this work
$Mn(3,5\text{-DBCat})_3^{2-}$	IV	1.891 (3)-1.922 (3)		27
$Mn(TPP)(OCH_3)_2$	IV	1.839 (2)	1.993 (3)-2.031 (3)	28

Table VIII. Bond Distances (Å) and Angles (deg) for the *trans*-$Mn[O_2C_6H_2(t\text{-Bu})_2]_2[NC_5H_5]_2$ Molecule

Inner Coordination Sphere			
Distances			
Mn-O(1)	1.854 (2)	Mn-N	2.018 (3)
Mn-O(2)	1.853 (2)		
Angles			
O(1)-Mn-O(2)	86.54 (9)	O(1)-Mn-N′	89.57 (10)
O(1)-Mn-O(2)′	93.45 (9)	O(2)-Mn-N	89.39 (11)
O(1)-Mn-N	90.43 (10)	O(2)-Mn-N′	90.61 (11)
3,5-DBCat Ligand			
Distances			
O(1)-C(1)	1.349 (4)	C(3)-C(4)	1.393 (5)
O(2)-C(2)	1.348 (4)	C(4)-C(5)	1.391 (5)
C(1)-C(2)	1.402 (4)	C(5)-C(6)	1.386 (4)
C(2)-C(3)	1.391 (4)	C(1)-C(6)	1.368 (4)
Angles			
Mn-O(1)-C(1)	111.5 (2)	O(1)-C(1)-C(6)	123.4 (3)
Mn-O(2)-C(2)	111.9 (2)	O(2)-C(2)-C(1)	114.7 (3)
O(1)-C(1)-C(2)	115.3 (3)	O(2)-C(2)-C(3)	125.0 (3)
Pyridine Ligand			
Distances			
N-C(15)	1.331 (4)	C(16)-C(17)	1.358 (6)
N-C(19)	1.325 (4)	C(17)-C(18)	1.362 (6)
C(15)-C(16)	1.351 (5)	C(18)-C(19)	1.372 (5)
Angles			
Mn-N-C(15)	120.6 (2)	C(15)-C(16)-C(17)	119.5 (4)
Mn-N-C(19)	121.7 (2)	C(16)-C(17)-C(18)	118.4 (4)
C(15)-N-C(19)	117.7 (3)	C(17)-C(18)-C(19)	119.3 (4)
N-C(15)-C(16)	122.9 (4)	C(18)-C(19)-N	122.1 (4)

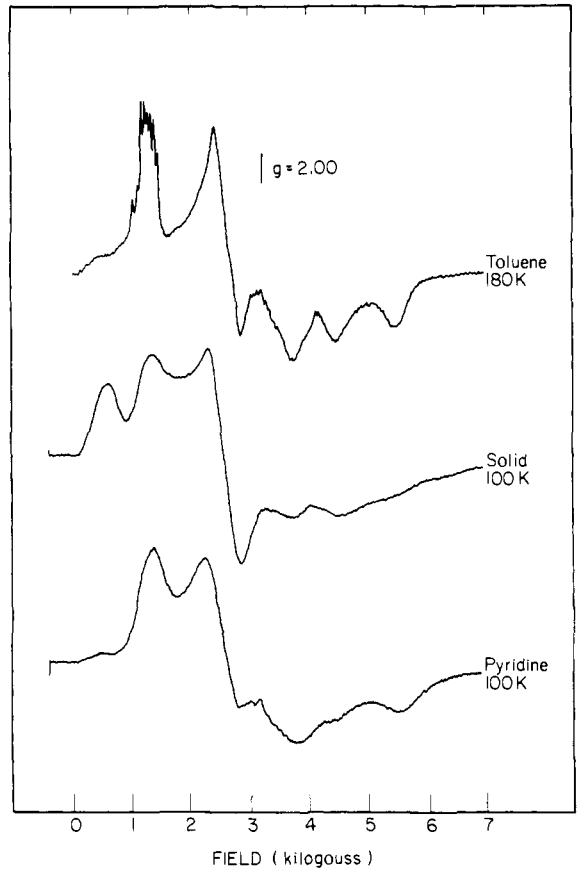

Figure 6. EPR spectra recorded on $Mn(3,5\text{-DBCat})_2(py)_2$ in various media.

complex is sensitive to the nature of other ligands bonded to the metal ion. Copper–quinone complexes illustrate this property in a clear way. With nitrogen donor ligands the copper–3,5-di-*tert*-butylquinone chelate ring consists of a Cu(II) metal ion and the quinone ligand bonded in the catecholate form (II). This is clear from the structural features of the complexes and their EPR spectra, which are typical of simple Cu(II) species.[33] Phosphorus donor ligands favor the Cu(I) form of the complex (III). The

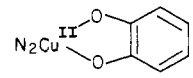

II, N_2 = bpy, phen, en

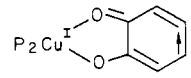

III, P_2 = diphos, $(PPh_3)_2$

EPR spectra of these complexes have *g* values that are close to 2.004, show strong coupling to ring protons, and show relatively weak coupling with the copper and phosphorus nuclei.[34] There is probably a structural change, from planar to tetrahedral, associated with the change in charge distribution.

The manganese–quinone chemistry contained in this report also illustrates the property of counterligand-dependent electronic structure. Pyridine is a stronger donor ligand than the bridging oxygen atoms of the $Mn_4(3,5\text{-DBSQ})_8$ tetramer. Filled Mn(II) d orbitals are raised in energy by addition of pyridine to the complex to the point where they are slightly above the semiquinone partially filled π^* levels. Two electrons localized on the metal ion in the tetramer move to the lower energy ligand-localized levels. This simple, qualitative description of the electronic changes which result from addition of pyridine ligands to the metal ion accounts for the reduction of the ligands with oxidation of the metal to Mn(IV).

A second effect observed in one case where the metal and ligand levels were quite close in energy is temperature-dependent electronic structure. An equilibrium between the cobalt(II)–semiquinone and cobalt(III)–catecholate forms of Co(3,5-DBSQ)(3,5-DBCat)(bpy) (eq 4) was observed over the range of tem-

$$Co^{III}(3,5\text{-DBSQ})(3,5\text{-DBCat})(bpy) \rightleftarrows Co^{II}(3,5\text{-DBSQ})_2(bpy) \quad (4)$$

perature between 240 and 340 K in toluene solution.[15] This also corresponds to the temperature range over which spectral changes were observed for $Mn(3,5\text{-DBCat})_2(py)_2$. Spectral data contained in Table IX together with the absence of an EPR spectrum for both the tetramer and the green form of the pyridine adduct point

(33) Buchanan, R. M.; Pierpont, C. G. *Inorg. Chem.*, submitted for publication.

(34) Razuvaev, G. A.; Cherkasov, V. K.; Abukumov, G. A. *J. Organomet. Chem.* **1978**, *160*, 361-371.

Table IX. Optical Spectra of Complexes containing Catecholate and Semiquinone Ligands

compd	solvent	λ_{max}, nm (ϵ, L mol^{-1} cm^{-1})
$Mn_4(3,5\text{-DBSQ})_8$	toluene	410 (4500), 760 (2500)
$Co_4(3,5\text{-DBSQ})_8$	toluene	380 (4800), 755 (2500)
$Ni_4(3,5\text{-DBSQ})_8$	toluene	430 (4500), 730 (2500)
$Cr(3,5\text{-DBSQ})_2(bpy)^+$	toluene	490 (7400), 522 (4700), 725 (2500)
$Co(3,5\text{-DBSQ})_2(bpy)$	toluene	550 (2000), 770 (2700)
$Ni(3,5\text{-DBSQ})_2(bpy)$	toluene	430 (4300), 765 (2500)
$Mn(3,5\text{-DBSQ})_2(py)_2$	toluene (299 K)	423, 781
$Mn(3,5\text{-DBCat})_2(py)_2$	toluene (232 K)	515, 824
	pyridine (240 K)	508, 833
$Mn(3,5\text{-DBCat})_3^{2-}$	CH_2Cl_2	585 (4500)

Table X. Metal Ion Oxidation States in $M(Q)_2(N\ donor)_2$ Complexes

metal	complex[a]	metal oxidation state	ref
Ni	$Ni(phenSQ)_2(py)_2$	II	30
	$Ni(3,5\text{-DBSQ})_2(bpy)$	II	30
Co	$Co(phenSQ)_2(py)_2$	II	30
	Co(3,5-DBSQ)(3,5-DBCat)(bpy)	III, II	15
Fe	Fe(phenSQ)(phenCat)(bpy)	III	35
	Fe(phenSQ)(phenCat)(phen)	III	35
	Fe(3,5-DBSQ)(3,5-DBCat)(bpy)	III	35
	Fe(3,5-DBSQ)(3,5-DBCat)(phen)	III	35
	Fe(3,5-DBSQ)(3,5-DBCat)(en)	III	35
Mn	$Mn(3,5\text{-DBCat})_2(py)_2$	IV, II	this work
Cr	Cr(phenSQ)(phenCat)(bpy)	III	36
	$Cr(Cl_4SQ)(Cl_4Cat)(bpy)$	III	36
	Cr(3,5-DBSQ)(3,5-DBCat)(bpy)	III	36

[a] Abbreviations used for quinone ligands: SQ = semiquinone, Cat = catecholate

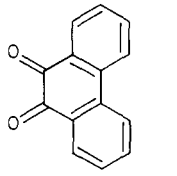

phenQ

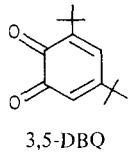

3,5-DBQ

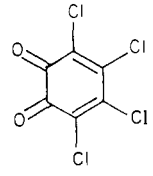

Cl_4Q

to a $Mn^{II}(SQ)_2$ charge distribution for the form of the adduct that exists in toluene solution at room temperature. The spectral change shown in Figure 5 would be associated with a $Mn^{II}(SQ)_2/Mn^{IV}(Cat)_2$ equilibrium (eq 5). As with cobalt the ox-

$$Mn^{IV}(3,5\text{-DBCat})_2(py)_2 \rightleftarrows Mn^{II}(3,5\text{-DBSQ})_2(py)_2 \quad (5)$$

idized metal form containing Mn(IV) prevails in solution at the lower region of the temperature range and also in the solid state at room temperature. In solution at higher temperatures the equilibrium shifts to favor the bis(semiquinone)manganese(II) form of the complex. There is no apparent evidence from our experimental results for a stable mixed-valence ligand Mn(III) complex $Mn(3,5\text{-DBSQ})(3,5\text{-DBCat})(py)_2$ as an intermediate.

The pyridine addition product $Mn(3,5\text{-DBCat})_2(py)_2$ is one member of a general series of complexes of form $M(Q)_2(N\ donor)_2$, where Q is a quinone ligand. Complexes listed in Table X have been prepared as simple adducts of oligomeric bis(semiquinone) complexes, by displacement of a quinone ligand from a tris(semiquinone) complex, or by using a reagent complex containing the nitrogen donor ligand.

$$M_4(SQ)_8 + 2(N\ donor) \rightarrow M(Q)_2(N\ donor)_2 \quad (6)$$

M = Mn, Co, Ni

$$Fe(SQ)_3 + 2(N\ donor) \rightarrow Fe(SQ)(Cat)(N\ donor)_2 \quad (7)$$

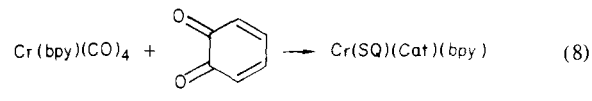

(8)

Metal ions used in these studies have extended across the first transition series, from Cr to Ni.[15,30,35,36] The quinone ligands in

Scheme I

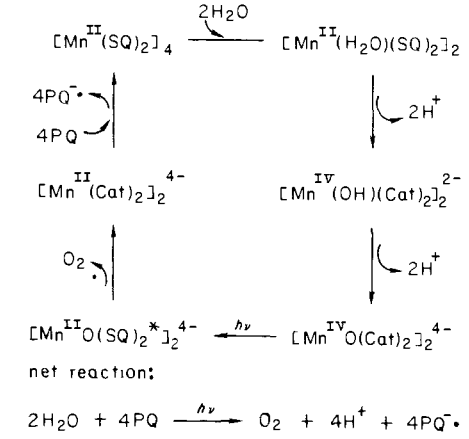

the complexes indicated above have been represented as Q without specifying charge because in moving from right to left across this series, from Ni to Mn, the degree of metal ion oxidation (and quinone ligand reduction) increases. Nickel complexes are bis(semiquinone)nickel(II) species, $Ni^{II}(SQ)_2(N\ donor)_2$. As mentioned earlier the cobalt complexes contain either Co(II) or Co(III) ions (eq 4). The iron complexes are exclusively (semiquinone)(catecholate)iron(III) species, $Fe(SQ)(Cat)(N\ donor)_2$, in the solid state. Continuing left, the manganese complex of this report exists as a bis(catecholate)manganese(IV) species in the solid state and in pyridine solution at room temperature. The chromium complexes represent a break in this pattern, resembling the iron series as $Cr(SQ)(Cat)(N\ donor)_2$ complexes. Related compounds prepared with vanadium and titanium have not yet been characterized.

Intramolecular Charge Separation in Manganese–Quinone Complexes and Its Relevance to Photosynthetic Water Oxidation. Model studies on metalloenzymes are often complicated by a paucity of specific information in the form of the biological metal complex and such is the case with the photosynthetic manganese protein. It is useful to compare unique properties of well-characterized, synthetic metal complexes to the biological system as functional models, and the ruthenium water oxidation system described by Meyer may provide useful information on requirements for water oxidation catalysts, both synthetic and biological.[3b,14] Characterization on the ruthenium system and on the biological manganese complex shows that the process leading to the production of O_2 can be broken down into two fundamental steps: (1) conversion of two water molecules to oxo ligands and (2) displacement of adjacent oxo oxygen atoms as O_2. This view focuses on changes that occur at the metal ions. Step 1 appears to occur with oxidation of the metals by two charge units each, Mn(II) to Mn(IV) in the photosynthetic system and Ru(III) to Ru(V) in the ruthenium dimer. The oxygen production step probably occurs with reduction of the metals to destabilize the oxo ligands and to restore the metal ions to their resting oxidation

(35) Lynch, M. W.; Valentine, M.; Hendrickson, D. N. *J. Am. Chem. Soc.* **1982**, *104*, 6982–6989.

(36) Buchanan, R. M.; Claflin, J.; Pierpont, C. G. *Inorg. Chem.* **1983**, *22*, 2552–2556.

state. The importance of this reduction step has been understated in consideration of models for the photosynthetic water oxidation system. To illustrate these points Scheme I shows how a manganese–semiquinone complex might function as a catalyst in a water oxidation system that uses a plastoquinone (PQ) as an electron acceptor. The scheme begins with a dimeric bis(semiquinone)manganese(II) complex which, in the initial step, forms an adduct by addition of two water molecules. Deprotonation of the aquo ligands is accompanied by transfer of two electrons from the metal to the quinone ligands, which affects oxidation of the metal *without oxidation of the complex unit*. Charge stored on the quinone ligands can later be returned to the metals in a photolytic ligand-to-metal charge-transfer step that leads to O_2 formation and reduction of the metal ions. The two-electron-transfer process and intense charge-transfer band in the visible spectrum of $Mn(3,5\text{-}DBCat)_2(py)_2$ demonstrate the feasibility of this step. Oxygen displacement leaves the Mn(II)–catecholate dimer $[Mn(Cat)_2]_2^{4-}$. This complex is similar to the product obtained by treating Mn(II) with 3,5-di-*tert*-butylcatechol, procedure 2 in the Experimental Section, which upon oxidation gives $Mn_4(3,5\text{-}DBSQ)_8$.

There is no evidence that the sequence of reactions outlined in this scheme is related specifically to steps in photosynthetic water oxidation. But the scheme shows how ligands that support reversible two-electron transfer with manganese can affect reversible intramolecular charge separation with the metal ions during the oxygen production process. It further suggests an interesting line of research for the manganese–quinone complexes.

Acknowledgment. Research carried out at the University of Colorado was supported by the NIH under Grant GM-23386. Work at the University of Illinois was funded by NIH Grant HL-13652.

Registry No. $Mn_4(O_2C_6H_2(t\text{-}Bu)_2)_8$, 78519-35-4; $Mn(O_2C_6H_4(t\text{-}Bu)_2)_2(NC_5H_5)_2{\cdot}2NC_5H_5$, 78470-59-4; $Mn^{II}(3,5\text{-}DBSQ)_2(py)_2$, 78470-58-3; $Mn_2(CO)_{10}$, 10170-69-1; H_2O, 7732-18-5; 3,5-di-*tert*-butyl-1,2-benzoquinone, 3383-21-9; 3,5-di-*tert*-butylcatechol, 1020-31-1.

Supplementary Material Available: Listing of structure factor amplitudes for the $Mn_4(3,5\text{-}DBSQ)_8$ and $Mn(3,5\text{-}DBCat)_2(py)_2$ structure determinations (17 pages). Ordering information is given on any current masthead page.

Crystal Structure and Magnetic Susceptibility of a Nonstoichiometric Tetranuclear Platinum Compound, *cis*-Diammineplatinum α-Pyrrolidone Green, $[Pt_4(NH_3)_8(C_4H_6NO)_4](NO_3)_{5.48}{\cdot}3H_2O$

Kazuko Matsumoto,* Hiromi Takahashi, and Keiichiro Fuwa

Contribution from the Department of Chemistry, Faculty of Science, University of Tokyo, Hongo, Bunkyo-ku, Tokyo 113, Japan. *Received July 20, 1983*

Abstract: From the reaction of the *cis*-dichlorodiammineplatinum hydrolysis product with α-pyrrolidone, crystals of *cis*-diammineplatinum α-pyrrolidone green (PPG) were obtained. Single-crystal X-ray diffraction analysis shows the compound consists of a tetranuclear chain cation, whose adjacent platinum atoms are bridged by α-pyrrolidone ligands. Each platinum atom is cis coordinated by two ammine ligands and either two exocyclic oxygen atoms or two deprotonated ring nitrogen atoms. The structure of the cation is basically identical with those of recently reported *cis*-diammineplatinum α-pyridone yellow (PPY), $[Pt_4(NH_3)_8(C_5H_4NO)_4](NO_3)_4$, blue (PPB), $[Pt_4(NH_3)_8(C_5H_4NO)_4](NO_3)_5{\cdot}H_2O$, and *cis*-diammineplatinum α-pyrrolidone tan (PPT), $[Pt_4(NH_3)_8(C_4H_6NO)_4](NO_3)_6{\cdot}2H_2O$. The Pt–Pt distances of PPG, 2.764 (8), 2.739 (8), 2.740 (8), 2.761 (8), 2.724 (8), and 2.753 (9) Å, are intermediate between those of PPB (2.7745 and 2.8770 Å) and PPT (2.702, 2.710, and 2.706 Å), which implies the average platinum oxidation state of PPG may be between those of PPB (2.25) and PPT (2.5). The magnetic susceptibility of PPG at 4.2–293 K obeys the Curie–Weiss law and the effective magnetic moment per tetranuclear platinum unit is 1.30 μ_B, which is far less than the value expected for the presence of one unpaired electron (1.73 μ_B). The low magnetic moment can be reasonably explained by assuming that PPG is a mixture of a PPB-corresponding paramagnetic five-charged cation and a PPT-corresponding diamagnetic six-charged cation. From the value of the measured magnetic moment, existence ratios of both cations were calculated as 52% for $[Pt_4(NH_3)_8(C_4H_6NO)_4]^{5+}$ and 48% for $[Pt_4(NH_3)_8(C_4H_6NO)_4]^{6+}$, and the average platinum oxidation state is 2.37. As a result, PPG is formulated as a nonstoichiometric compound, $[Pt_4(NH_3)_8(C_4H_6NO)_4](NO_3)_{5.48}{\cdot}3H_2O$.

Recently, a series of platinum compounds called "platinum blues" have attracted the interest of chemists because of their unusual dark blue color and high antitumor activities.[1-3] Efforts have been made to characterize them chemically[4] and spectroscopically,[5,6] however, with only a little definite conclusion that they are paramagnetic and oligomeric.

A recent breakthrough for the study of this class of compounds is the single-crystal X-ray diffraction study of *cis*-diammineplatinum α-pyridone blue (PPB), $[Pt_4(NH_3)_8(C_5H_4NO)_4](NO_3)_5{\cdot}H_2O$.[7,8] The compound consists of a tetranuclear chain

(1) Hofmann, K. A.; Bugge, G. *Chem. Ber.* **1908**, *41*, 312–334.
(2) Brown, D. B.; Burbank, R. D.; Robin, M. B. *J. Am. Chem. Soc.* **1969**, *91*, 2895–2902.
(3) Davidson, P. J.; Faber, P. J.; Fischer, R. G., Jr.; Mansy, S.; Peresie, H. J.; Rosenberg, B.; Van Camp, L. *Cancer Chemother. Rep.* **1975**, *59*, 287–300.
(4) Flynn, C. M., Jr.; Viswanathan, T. S.; Martin, R. B. *J. Inorg. Nucl. Chem.* **1977**, *39*, 437–439.
(5) Lippert, B. J. *Clin. Hematol. Oncol.* **1977**, *7*, 26–50.
(6) Macfarlane, R. D.; Torgensen, D. F. *Science* **1976**, *191*, 920–925.
(7) Barton, J. K.; Rabinowitz, H. N.; Szalda, D. J.; Lippard, S. J. *J. Am. Chem. Soc.* **1977**, *99*, 2827–2829.
(8) Barton, J. K.; Szalda, D. J.; Rabinowitz, H. N.; Waszczak, J. V.; Lippard, S. J. *J. Am. Chem. Soc.* **1979**, *101*, 1434–1441.

0002-7863/84/1506-2049$01.50/0